Electronic Supplementary Material (ESI) for ChemComm.


# Supporting Information

## P3-type Layered $K_{0.48}Mn_{0.4}Co_{0.6}O_2$: A Novel Cathode Material for Potassium-Ion Battery

Krishnakanth Sada and Prabeer Barpanda*

*Faraday Materials Laboratory, Materials Research Centre, Indian Institute of Science, C.V. Raman Avenue, Bangalore, 560012, India.*

* author for correspondence
E-mail: prabeer@iisc.ac.in
Phone: +91-80 2293 2783; Fax: +91-80 2360 7316

**Synthesis procedure**: Stoichiometric amounts of $KNO_3$, $MnCO_3$ and $Co_3O_4$ precursors [in molar ratio K: Co: Mn = 1: 0.6: 0.4] were intimately mixed by wet planetary milling for 30 mins using acetone media. This mixture was pelletized by applying uniaxial hydraulic pressure (10 MPa). These pellets were annealed at 800 °C for 12 h (in air). The annealed product was quenched directly to room temperature and was transferred to an argon-filled glove box. Crystal structure of the as-synthesized blackish-brown powder product was analysed by X-ray diffraction with a PANalytical X'pert pro diffractometer equipped with Cu Kα1 (λ = 1.54 Å) radiation source with Ni-filter acting as a monochromator.

Careful preparation and handling of cathode materials is crucial to obtain robust electrochemical cyclability in case of potassium-ion batteries. Firstly, we prepared our electrodes by solid-state route having specific composition of K: Mn: Co = 0.48: 0.4: 0.6. It was homogeneously mixed with teflonized acetylene black (TAB) in 8:2 ratio resulting in sheets of few micron thickness, which were used as working electrode. The preparation of the electrodes was carried inside an Ar-filled glove box (with low ppm level of $O_2$ <0.5 and $H_2O$ <0.5) to avoid contamination/ decomposition of material from moisture adsorption. As the potassium-based cathode materials are highly sensitive to air/ moisture, it is crucial to handle the electrode and assemble battery in inert atmosphere. This is the major reason behind the high capacity retention in the present study. Further, these cathode sheets were found to be intact after cycling as observed from the high-intensity ex-situ XRD peaks.

From structural point-of-view, substitution of high percentage of Co in K-Mn-O ternary mixture is beneficial for structural stability. In case of Na-based Co-Mn bimetallic compositions, formation of a stable passivating layer at the electrode interface has been reported. It is more favorable for higher degree of Co substitution in the lattice. This substitution does not affect the structural lattice because of similar ionic radii of Co and Mn ($Co^{4+}$= 0.53 Å and $Mn^{4+}$= 0.53Å).

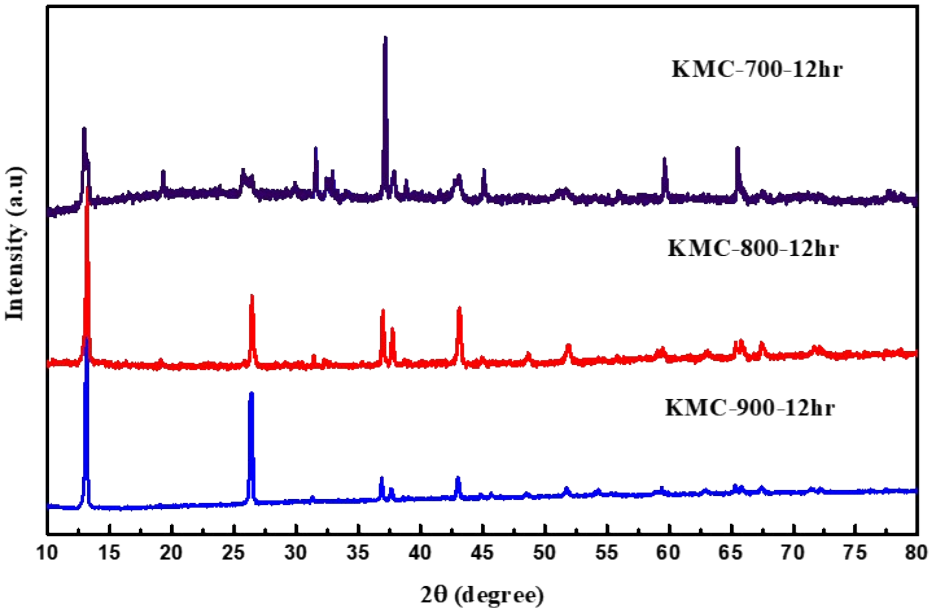


**Figure S1**: Solid-state synthesis of $K_{0.48}Mn_{0.4}Co_{0.6}O_2$ (KMC) cathode prepared by annealing at three different temperature (from 700 ~ 900 °C for 12 h).

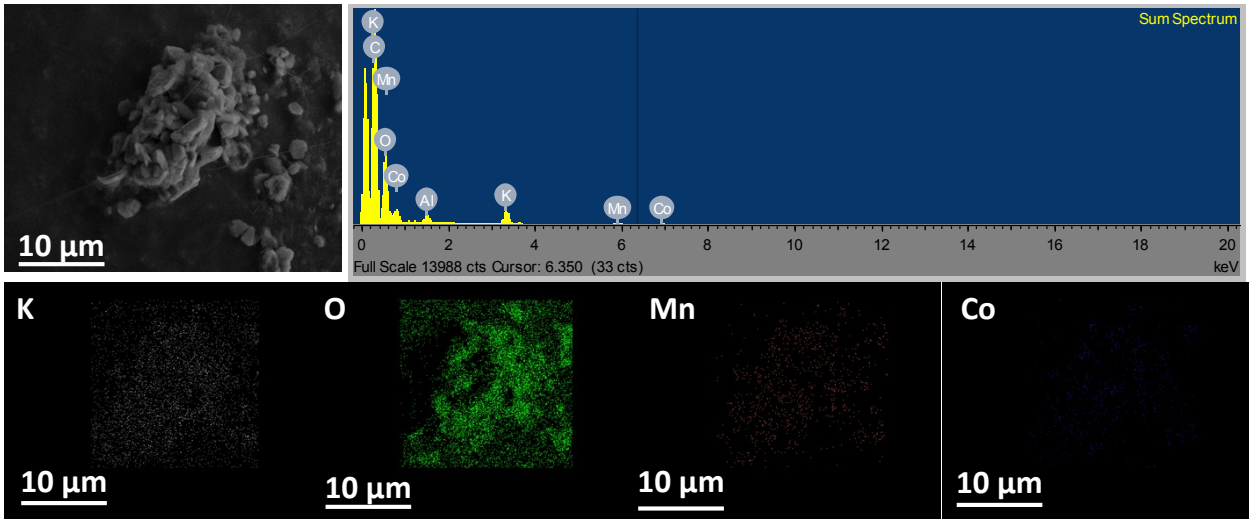


**Figure S2**: Representative SEM micrograph, energy dispersive spectrum and elemental mapping in pristine $K_{0.48}Mn_{0.4}Co_{0.6}O_2$ (KMC) cathode material.

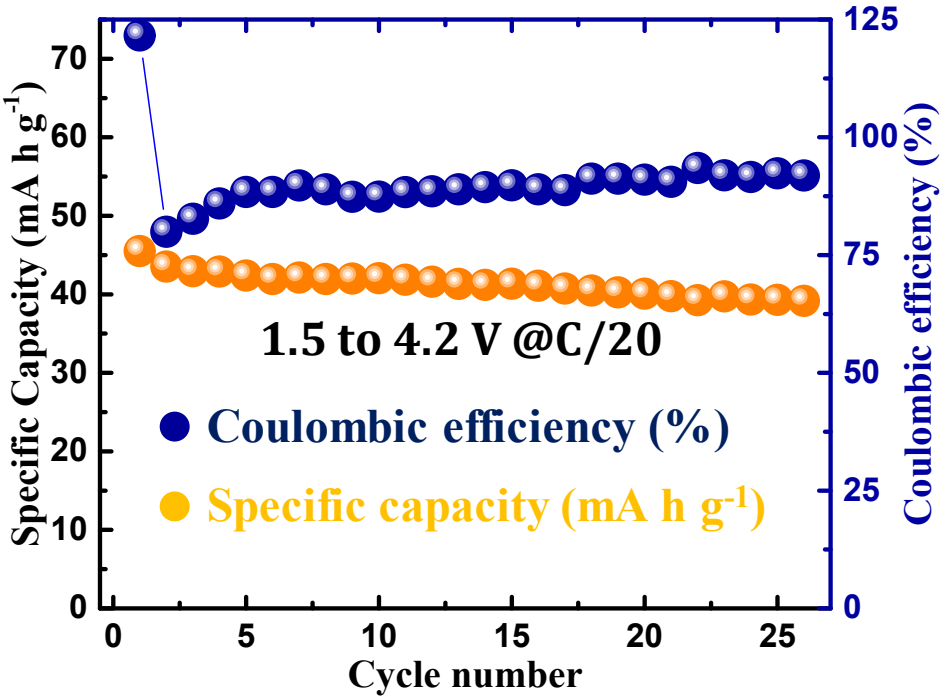


**Figure S3**: Cycling stability at current rate of C/20 in potential window of 1.5 to 4.2 V.

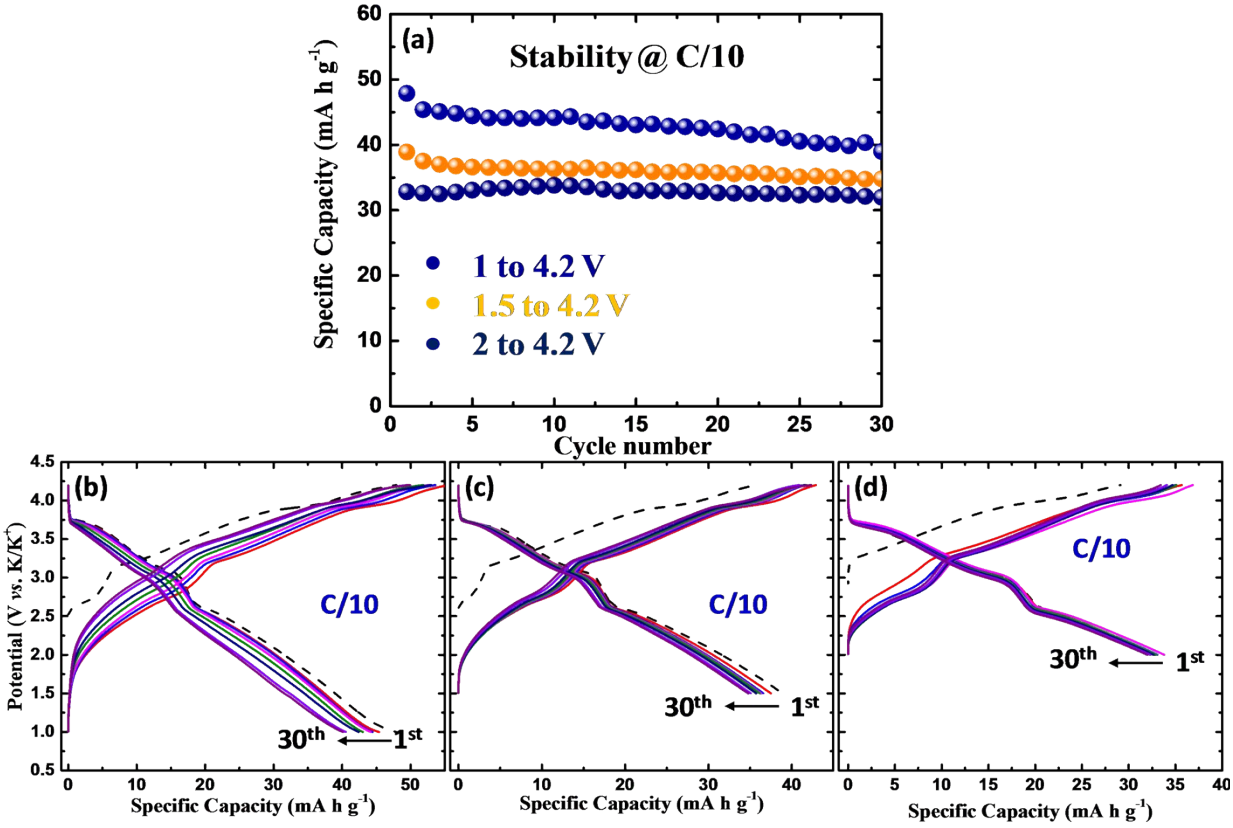


**Figure S4**: (a) Cycling stability over initial 30 cycles perfomed in three different potential windows. Galvanostatic (dis)charge voltage curves of $K_{0.48}Mn_{0.4}Co_{0.6}O_2$ (KMC) cathode (cycled at the rate of C/10 in three different electrochemical windows of (b) 1 to 4.2 V, (c) 1.5 to 4.2 V and (d) 2 to 4.2 V.

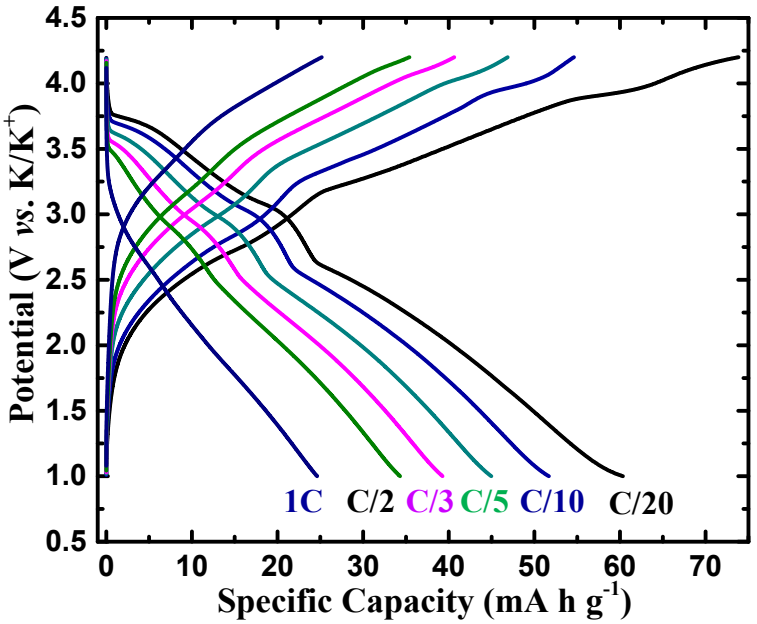


**Figure S5**: Comparative (dis)charge voltage profiles of second cycles at different current rates (from C/20 to 1C rate).

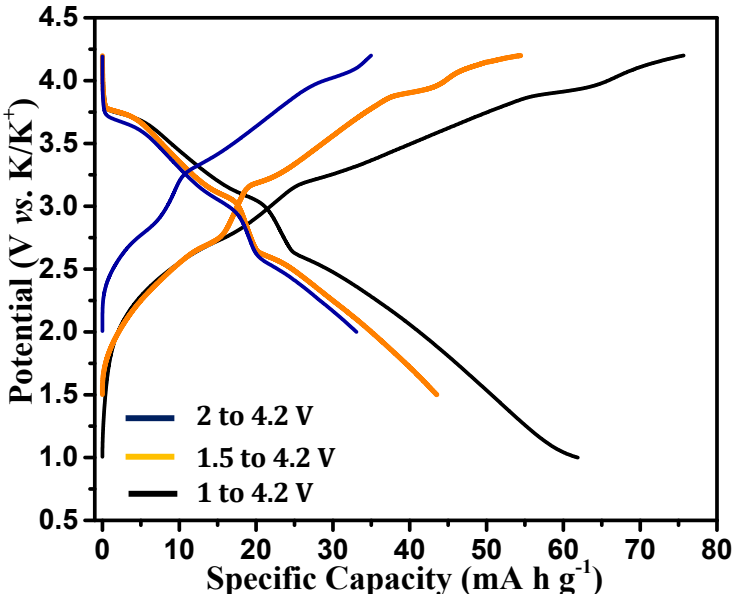


**Figure S6**: Comparison of charge/discharge plots carried in three different potential ranges at a current rate of C/20.

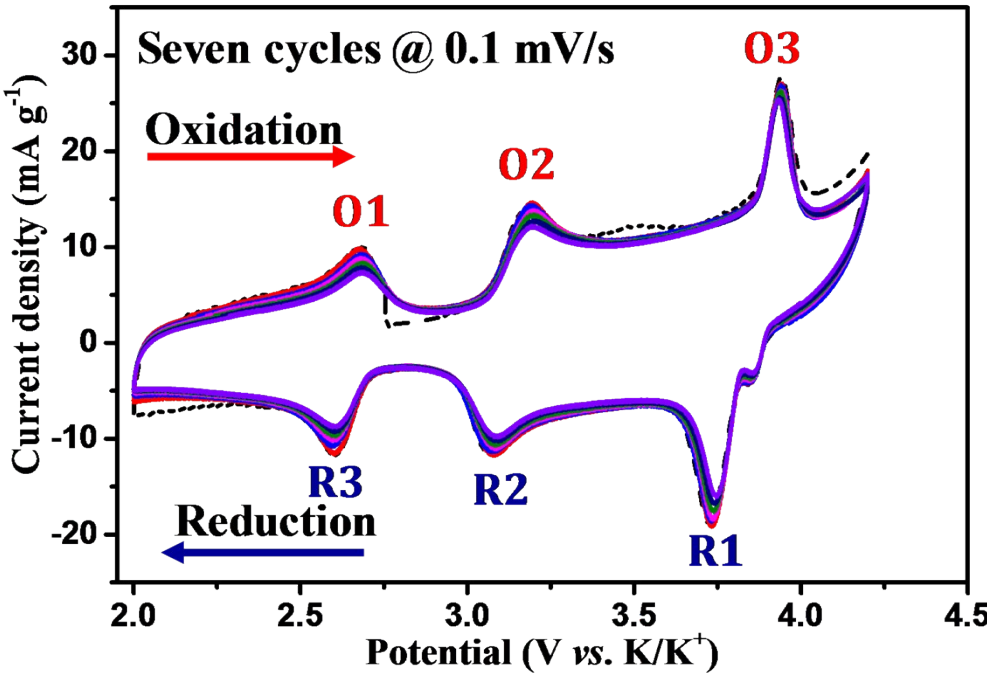


**Figure S7**: Cyclic voltammogram of $K_{0.48}Mn_{0.4}Co_{0.6}O_2$ (KMC) cathode at a scan rate of 0.1 mV/s.

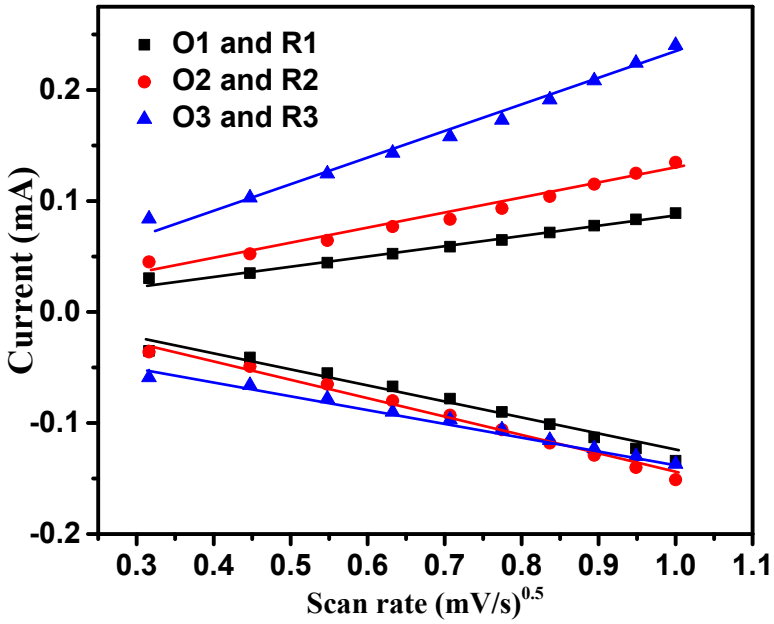


**Figure S8:** Peak current ($I_p$) vs. square root ($v^{0.5}$) of the scan rate for both anodic and cathodic process during cyclic voltammetry of $K_{0.48}Mn_{0.4}Co_{0.6}O_2$ (KMC) cathode.

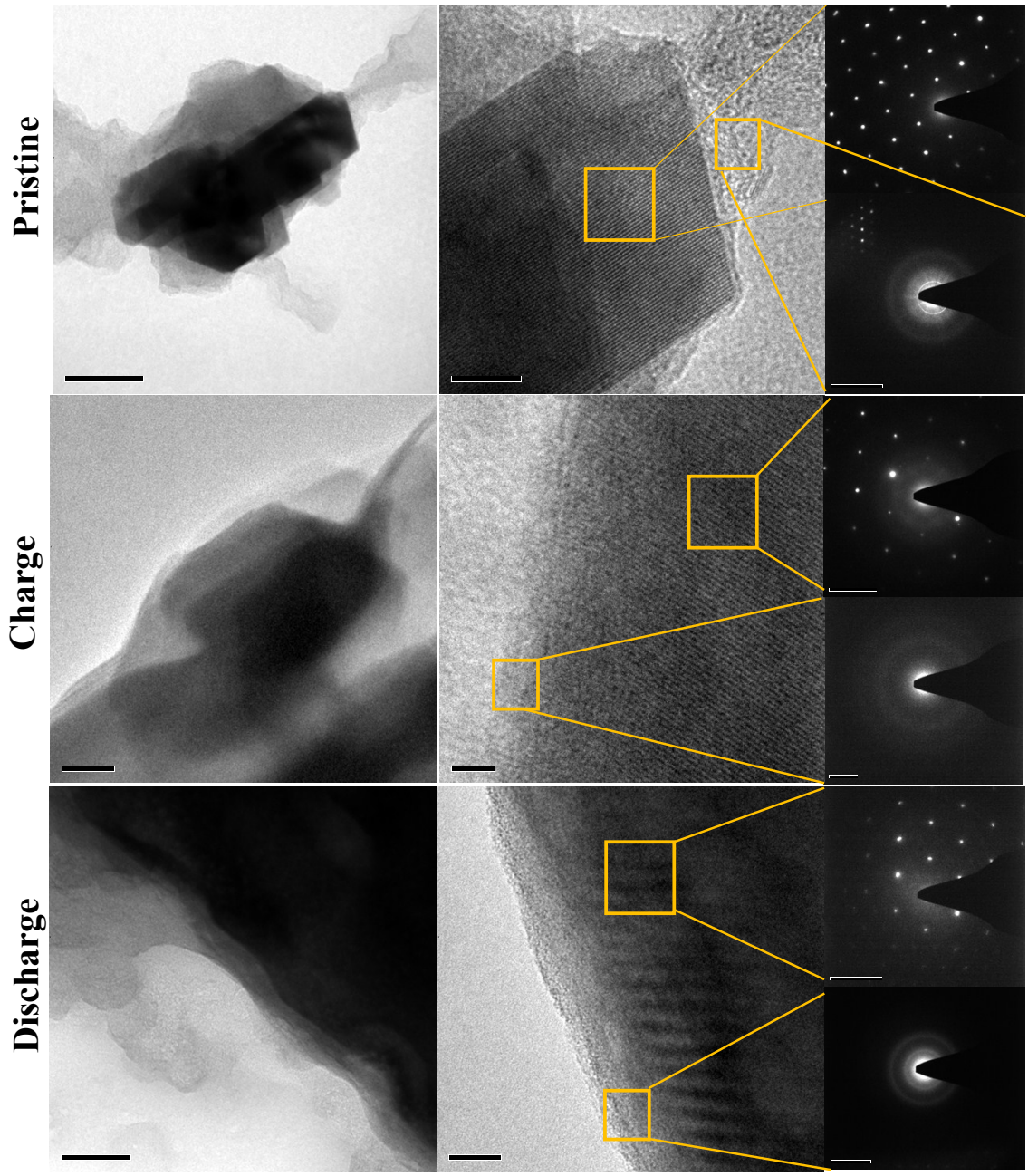


**Figure S9**: Detailed TEM analysis of the pristine, charged and discharged electrodes.

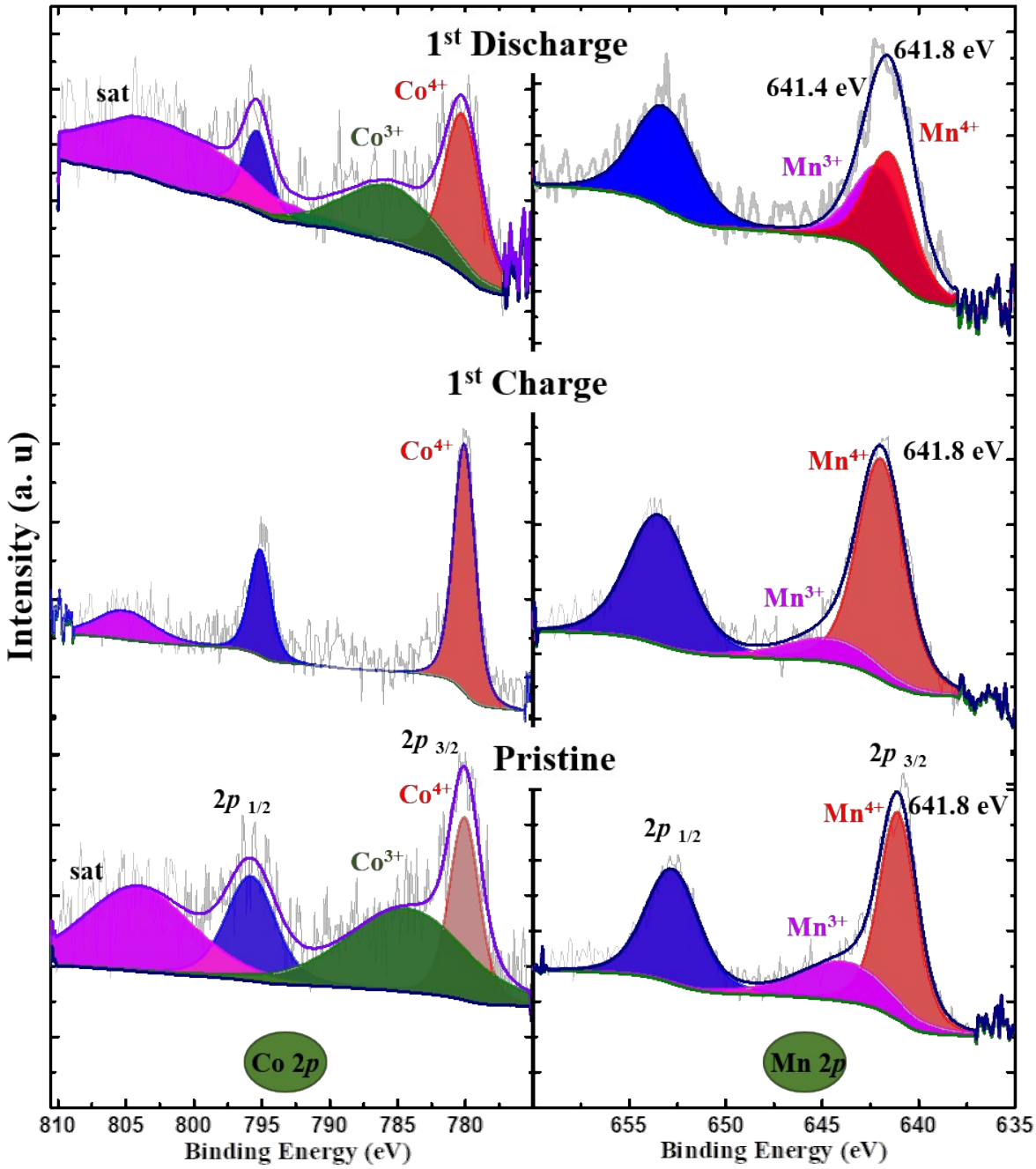


**Figure S10**: XPS analysis: The Co and Mn oxidation states are compared upon the (dis)charge with pristine (2p orbitals) cathode. Variation in valency states is observed for both Co and Mn. The Co 2p (810-775 eV) having satellite peaks feature in both pristine and discharged states. It implies the presence of $Co^{4+}/Co^{3+}$ mixed oxidation state. Upon charging, the electrode oxidation state changed to have exclusively $Co^{4+}$. In case of Mn (660-635 eV), both pristine and discharged electrode have Mn 2p 3/2 located at 641.8 eV corresponding to 4+ oxidation state. After charge, it showed $Mn^{4+}/Mn^{3+}$ mixed oxidation state. The partial reduction of Mn implies the stability of the structure upon the (dis)charge steps.

**Table S1.** Comparative electrochemical performance of various cobalt and manganese-based oxide cathode materials for potassium-ion batteries (KIBs).

| Sl. No. | Material | Specific Capacity (mA h $g^{-1}$) | Current Rate (mA $g^{-1}$) | Average potential (V) | Voltage window (V) | Ref. |
|---|---|---|---|---|---|---|
| 1. | $Na_{0.84}CoO_2$ | 82 | C/20 | 3.2 | 2.0-4.2 | 1 |
| 2. | $K_{0.41}CoO_2$ | 60 | 11.8 | 3.1 | 2.0-3.9 | 2 |
| 3. | $K_{0.6}CoO_2$ | 78 | C/40 | 2.7 | 1.5-3.9 | 3 |
| 4. | $K_{0.6}CoO_2$ | 82 | 10 | 2.8 | 1.7-4.0 | 4 |
| 5. | $Na_2Mn_3O_7$ | 152 | C/20 | 2.1 | 1.5-3.0 | 5 |
| 6. | $K_{0.3}MnO_2$ | 74 | C/10 | 2.6 | 1.5-3.5 | 6 |
| 7. | $K_{0.5}MnO_2$ | 100 | 5 | 2.6 | 1.5-3.9 | 7 |
| 8. | $K_{0.3}Mn_{0.95}Co_{0.05}O_2$ | 99 | 22 | 2.5 | 2.0-3.6 | 8 |
| 9. | $K_{0.67}Ni_{0.17}Co_{0.17}Mn_{0.66}O_2$ | 76 | 20 | 3.1 | 2.0-4.3 | 9 |
| 10. | $K_{0.65}Fe_{0.5}Mn_{0.5}O_2$ | 151 | 20 | 2.5 | 1.5-4.2 | 10 |
| 11. | $K_{0.6}Ni_{1/3}Co_{1/3}Te_{1/3}O_2$ | 30 | C/20 | 4.1 | 1.2-4.5 | 11 |
| 12 | $K_{0.45}Mn_{0.5}Co_{0.5}O_2$ | 89 | 10 | 2.55 | 1.5-3.9 | 12 |
| **13.** | **$K_{0.48}Mn_{0.4}Co_{0.6}O_2$** | **64** | **C/20** | **3** | **1.0-4.2** | **This work** |

**Reference:**


1 K. Sada, B. Senthilkumar and P. Barpanda, *Chem. Commun.*, 2017, **53**, 8588-8591.

2 Y. Hironaka, K. Kubota and S. Komaba, *Chem. Commun.*, 2017, **53**, 3693-3696.

3 H. Kim, J. C. Kim, S. H. Bo, T. Shi, D. H. Kwon and G. Ceder, *Adv. Energy Mater.*, 2017, **7,** 1700098.

4 T. Deng, X. Fan, C. Luo, J. Chen, L. Chen, S. Hou, N. Eidson, X. Zhou and C. Wang, *Nano Lett.*, 2018, **18**, 1522-1529.

5 K. Sada, B. Senthilkumar and P. Barpanda, *ACS Appl. Energy Mater.*, 2018, **1**, 5410-5416.

6 C. Vaalma, G. A. Giffin, D. Buchholz and S. Passerini, *J. Electrochem. Soc.*, 2016, **163**, A1295-A1299.

7 H. Kim, D. H. Seo, J. C. Kim, S. H. Bo, L. Liu, T. Shi and G. Ceder, *Adv. Mater.*, 2017, **29**, 1702480.

8 Q. Zhang, C. Didier, W. K. Pang, Y. Liu, Z. Wang, S. Li, V. K. Peterson, J. Mao and Z. Guo, *Adv. Energy Mater.*, 2019, **9**, 1900568.

9 C. Liu, S. Luo, H. Huang, Z. Wang, A. Hao, Y. Zhai and Z. Wang, *Electrochem. Commun.*, 2017, **82**, 150-154.

10 T. Deng, X. Fan, J. Chen, L. Chen, C. Luo, X. Zhou, J. Yang, S. Zheng and C. Wang, *Adv. Funct. Mater.*, 2018, **28**, 1800219.

11 T. Masese, K. Yoshii, M. Kato, K. Kubota, Z.-D. Huang, H. Senoh and M. Shikano, *Chem. Commun.*, 2019, **55**, 985-988.

12 H. V. Ramasamy, B. Senthilkumar, P. Barpanda and Y.-S. Lee, *Chem. Eng. J.*, 2019, **368**, 235-243.